ISSN (Print) 1226-1750
ISSN (Online) 2233-6656
Journal of Magnetics 24(4), 725-728 (2019) https://doi.org/10.4283/JMAG.2019.24.4.725

Design of a Depth of Interaction Detector Module for Use in a Magnetic Resonance Imaging System

Seung-Jae Lee[1,2] and Cheol-Ha Baek[3]*

[1]*Department of Radiological Science, Dongseo University, Busan 47011, Republic of Korea*
[2]*Center for Radiological Environment & Health Science, Dongseo University, Busan 47011, Republic of Korea*
[3]*Department of Radiological Science, Kangwon National University, Gangwon 25949, Republic of Korea*

(Received 1 November 2019, Received in final form 10 December 2019, Accepted 11 December 2019)

In this study, we designed a depth of interaction (DOI) detector module for use in a magnetic resonance imaging (MRI) system. The detector uses a semiconductor photosensor that is unaffected by a magnetic field. The detector module consists of two layers of a crystal array that have different light sharing characteristics. To verify the performance of the detector module, simulations of the optical photon transport in the crystal array were performed with a DETECT2000 tool. Various combinations of the parameters, such as the reflector used and the treatment of crystal surfaces, were simulated and the characteristics were evaluated through a reconstructed flood image. In certain combinations of the simulation conditions, all of the crystal pixels could be identified along all directions. Thus, the proposed DOI detector module could extract the three-dimensional gamma ray interaction position from the two-dimensional flood image.

Keywords : Depth of interaction, PET/MRI, surface treatment, DETECT2000

1. Introduction

Preclinical studies are increasing the interest in the use of positron emission tomography (PET) for studies on small animals for demonstrating biomedical mechanisms [1]. In vivo molecular imaging on small animals requires dedicated PET scanners for high resolution and sensitivity. PET can provide the position of concentrations of a labeled molecule, but is poor at providing anatomical structures. PET has been combined with other techniques, such as computed tomography (CT) or magnetic resonance imaging (MRI), to provide an anatomical backdrop, which has increased the value of PET [2, 3]. When PET/MRI and PET/CT have been used for preclinical studies, PET generally has had a small ring diameter and thin, long scintillation crystals for high resolution and sensitivity. However, the spatial resolution of a system using thin, long crystals gradually degrades from the center to the periphery of the field of view (FOV) because of the increase in the fraction of gamma rays obliquely incident on the detector surface [4-6]. The measurement of the depth of interaction (DOI) within the crystals is an effective way to enhance the spatial resolution and uniformity in the FOV [7]. Many DOI measurement methods have been developed, including multi-layer detectors, direct measuring detectors, dual-ended readout detectors, and detectors using a wavelength-shifting fiber [8-12].

In this study, we designed a novel DOI detector module for use in an MRI system. The module consisted of two crystal layers. Different treatments were applied to the surfaces of the crystals in the top and bottom layers in order to separate the imaging positions. The top layer shared a significant amount of light generated by the interaction with gamma rays, but the bottom layer shared little light because of reflectors. To verify the performance of the detector module, simulations were performed with a DETECT2000 tool [13].

2. Experimental Details

2.1. Configuration of the DOI detector module

The detector module is composed of two layers of gadolinium aluminum gallium garnet (GAGG) crystal arrays [14] and photosensor arrays, as shown in Fig. 1. GAGG, which has a similar density and excellent scintillation characteristics, was chosen as the scintillator

*Corresponding author: Tel: +82-33-540-3389
Fax: +82-33-540-3389, e-mail: baekch100@gmail.com

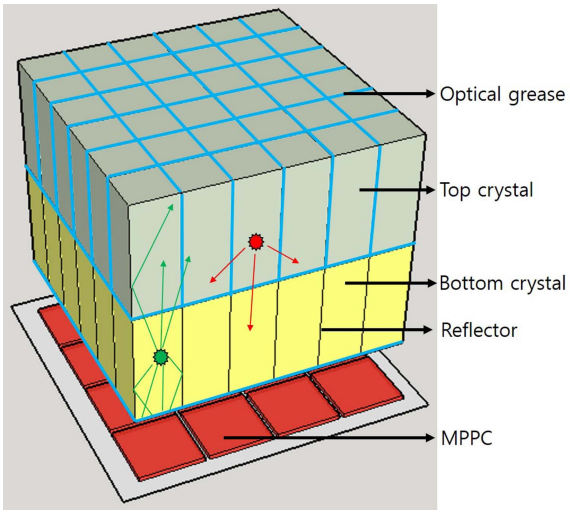

Fig. 1. (Color online) Geometry of the DOI detector module for use in an MRI system. The sky blue lines represents the optical grease that was used to optically couple the crystal-crystal and crystal-MPPC combinations. The light generated in the top crystals was easy to move to other crystals, but the light generated in the bottom crystals was relatively more difficult to move. The red star represents the gamma interaction position, and each color line represents the direction of light movement.

of the detector. The light generated from the top crystals is easy to move to other crystals because the crystals are optically coupled to each other with optical grease, but the light of the bottom crystals is relatively difficult to move because of the treatment of the reflectors. The light emission of the GAGG crystal is 57,000 photons/MeV and shows a peak emission of 520 nm. The GAGG crystal array in each layer consists of 6 × 6 crystals, each with dimensions of 2 × 2 × 5 mm^3. The photosensor uses a Hamamatsu multi-pixel photon counter (MPPC) array (S13361-3050 series) [15]. Because the MPPC as a semiconductor photosensor is not affected by a magnetic field, it can be used in an MRI system. The MPPC array is made up of 4 × 4 pixels, with each pixel having a photosensitive area of 3 × 3 mm^2 and the sensors having a pitch of 3.2 mm. The MPPC has a spectral response in the range of 320-900 nm with a peak sensitivity wavelength at 450 nm (40 % quantum efficiency). The quantum efficiency of the crystal peak emission is approximately 35 %.

2.2. Simulation conditions

All side surfaces of the GAGG crystal in the bottom layer (refractive index: 1.90) were treated with reflectors, such as METAL as a specular reflector with a reflection coefficient (RC) of 0.98, and PAINT as a diffuse reflector, also with an RC of 0.98. The other surfaces were optically coupled to the top crystal layer and the MPPC array. The outermost side and top surfaces of the top crystal array were treated as a reflector, either METAL or PAINT, and the others were optically connected to each other. The coupling material used optical grease (refractive index: 1.465) so that light could be shared and directed. The MPPC was treated with epoxy resin (refractive index: 1.55) as a detection surface. The optically coupled surfaces of the crystals were simulated with POLISH as a polished surface and GROUND as a rough surface. Table 1 summarizes the simulation conditions.

Table 1. Simulation conditions for the DOI detector module. Reflector parameters use METAL as a specular reflector and PAINT as a diffuse reflector, both of which had a reflector coefficient of 98 %. The crystal surfaces were treated with GROUND as a rough surface and POLISH as a polished surface. Because the side and bottom surfaces in the top layer crystals were optically coupled, the parameter combinations of each surface were treated independently.

Conditions	Reflector		Crystal Surface		
	Top	Bottom	Top side	Top bottom	Bottom
Case 1	METAL	METAL	GROUND	GROUND	GROUND
			GROUND	POLISH	POLISH
			POLISH	POLISH	POLISH
			POLISH	GROUND	GROUND
Case 2	PAINT	PAINT	GROUND	GROUND	GROUND
			GROUND	POLISH	POLISH
			POLISH	POLISH	POLISH
			POLISH	GROUND	GROUND

The 511 keV gamma ray interactions were generated at the center of each crystal, with a total of 1,000 simulated gamma events. The number of light photons generated by the gamma ray interaction was determined from the light yield of GAGG crystal for a 511 keV gamma ray combined with the quantum efficiency of the MPPC.

3. Results and Discussion

The light generated from the central position of each crystal in the top and bottom layers was acquired from the MPPC of 16-channels, and these signals were reduced to 4-channels to make the same number of data processing channels used in a general PET detector. 4-channel signals were reconstructed as a flood image using the Anger equation (1).

$$X\ position = \frac{X^+ - X^-}{X^+ + X^-},\ Y\ position = \frac{Y^+ - Y^-}{Y^+ + Y^-} \quad (1)$$

Figure 2 and 3 illustrate representative flood images

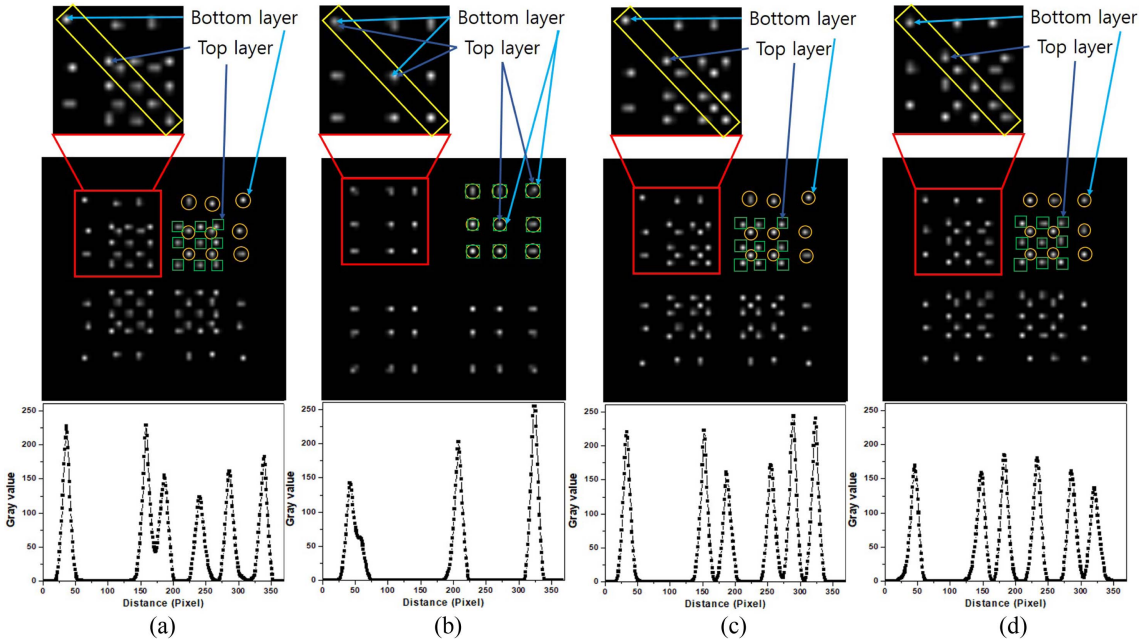

Fig. 2. (Color online) The flood image and row profiles for various combinations of crystal surfaces when using the METAL reflector. (a) All crystal surfaces were treated with GROUND. (b) All crystal surfaces were treated with POLISH. (c) The side surfaces of the crystal were treated with POLISH and the bottom surfaces were treated with GROUND in the top layer. (d) The side surfaces of the crystal were treated with GROUND and the bottom surfaces were treated with POLISH in the top layer.

and row profiles in various combinations of the simulation conditions. Depending on the coupled characteristics of the crystals and MPPCs, each image appeared symmetric relative to the center. Figure 2 shows images obtained from various surface treatments of crystals, such as all GROUND (a), all POLISH (b), and one GROUND and the other POLISH (c, d), when the METAL reflector is used. Figure 2 is symmetrical with four parts, one of

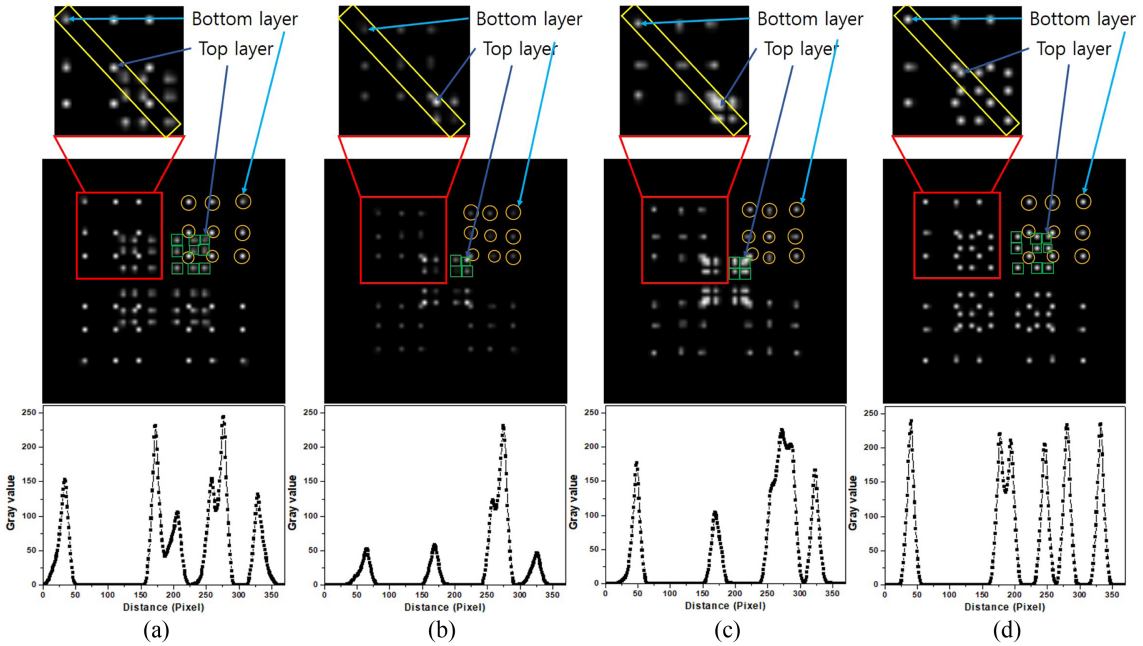

Fig. 3. (Color online) The flood image and row profiles in various combinations of crystal surfaces when using the PAINT reflector. (a) All crystal surfaces were treated with GROUND. (b) All crystal surfaces were treated with POLISH. (c) The side surfaces of the crystals were treated with POLISH and the bottom surfaces of the crystal were treated with GROUND in the top layer. (d) The side surfaces of the crystal were treated with GROUND and the bottom surfaces were treated with POLISH in the top layer.

which is enlarged. The profile of the yellow box area was obtained and is shown in the lower part of the figure. All the crystal pixels are identified along the X, Y, and depth directions in Figure 2(a), (c), and (d), but not in Figure 2(b), which is also verified in the profiles. Figure 3 shows the flood images and profiles when using the PAINT reflector, and the surface treatments of the crystal were the same as in Figure 2. The crystal pixels are identified along the X, Y, and depth directions in Figure 3(a), (d), but those were not perfect. Figure 3(b), (c) show that the X, Y, and depth directions were not separated, and the crystal pixels of the top layer were imaged in the center more than in the other images. In Figures 2 and 3, it can be seen that the crystal pixels are more clearly separated when the reflector used was METAL rather than PAINT. When the side surface of the top layer crystal pixels was treated with GROUND, the identification was better than when they were treated with POLISH. The combination of the simulation parameters that showed the best discrimination ability was when the side and bottom surfaces of the top layer crystals were treated differently, with one treated with GROUND and the other treated with POLISH, combined with the METAL reflector.

4. Conclusion

We designed a DOI detector module consisting of a two layer crystal array for use in an MRI system. The crystal side surfaces of the bottom layer were all treated with reflectors to limit the sharing of light, and the top layers were configured so that the reflectors were partially used to allow significant light sharing with other crystals. The simulation was performed using various combinations of the parameters such as the specular and diffuse reflectors and the polished and rough surfaces of the crystals, and the flood image was reconstructed with the acquired data. All the crystal pixels in the flood image could be identified along all directions in particular combinations of the simulation conditions. The parameter combinations that yielded the best characteristics were the METAL reflector combined with the side and bottom of the top layer crystal surfaces having different treatments. These results are promising for the design of a preclinical PET/MRI system for high resolution because the proposed DOI detector module can extract the 3-dimensional gamma ray interaction position from the 2-dimensional flood image without being affected by the magnetic field.

Acknowledgment

This research was supported by the National Foundation of korea (NRF) funded by the Ministry of Education, Science and Technolgoy (2018R1C1B5085189).

References

[1] Hao Peng and Craig S. Levin, Curr. Pharm. Biotechnol. **11**, 6 (2010).
[2] Keiichi Magota, NaoKi Kubo, Yuji Kuge, Ken-ichi Nishijima, Songji Zhao, and Nagara Tamaki, Eur. J. Nucl. Med. Mol. Imaging **38**, 4 (2011).
[3] Kálmán Nagy, Miklós Tóth, Péter Major, Gergely Patay, Gyözö Egri, Jenny Häggkvist, Andrea Varrone, Lars Farde, Christer Halldin, and Balázs Gulyás, J. Nucl. Med. **54**, 10 (2013).
[4] R. S. Miyaoka, T. K. Lewellen, H. Yu, and D. L. McDaniel, IEEE Trans. Nucl. Sci. **45**, 3 (1998).
[5] W. W. Moses, Nucl. Inst. Meth. A **648**, Supplement 1 (2011).
[6] M. Ito, S. J. Hong, and J. S. Lee, Biomed. Eng. Lett. **1** (2011).
[7] L. R. MacDonald and M. Dahlbom, IEEE Trans. Nucl. Sci. **45**, 4 (1998).
[8] J. H. Jung, Y. Choi, Y. H. Chung, O. Devroede, M. Krieguer, P. Bruyndonckx, and S. Tavernier, Nucl. Inst. Meth. A **571** (2007).
[9] A. Vandenbroucke, A. M. K. Foudray, P. D. Olcott, and C. S. Levin, Phys. Med. Biol. **55**, 19 (2010).
[10] Y. Shao, R. W. Silverman, R. Farrell, L. Cirignano, R. Grazioso, K. S. Shah, G. Visser, M. Clajus, T. O. Tumer, and S. R. Cherry, IEEE Trans. Nucl. Sci. **47**, 3 (2000).
[11] S-J. Lee and C-H. Baek, Nucl. Inst. Meth. A **887** (2018).
[12] S-J. Lee and C-H. Baek, J. Magnetics **23**, 4 (2018).
[13] F. Cayouette, D. Laurendeau, and C. Moisan, Proceeding SPIE, **4833** (2003).
[14] http://www.furukawa-denshi.co.jp/cgi-bin/pdfdata/20140428162950.pdf
[15] https://www.hamamatsu.com/resources/pdf/ssd/s13361-3050_series_kapd1054e.pdf